Available online at www.sciencedirect.com
SCIENCE DIRECT®
Journal of Catalysis 223 (2004) 142–151
JOURNAL OF CATALYSIS
www.elsevier.com/locate/jcat

Kinetics of the CO + N_2O reaction over noble metals II. Rh/Al_2O_3 and $Pt–Rh/Al_2O_3$

P. Granger,* P. Malfoy, and G. Leclercq

Université des Sciences et Technologies de Lille, Laboratoire de Catalyse de Lille, UMR CNRS No. 8010, Bât. C3, 59655 Villeneuve d'Ascq cedex, France

Received 17 July 2003; revised 24 November 2003; accepted 13 January 2004

Abstract

The subsequent reduction of N_2O by CO is an important subreaction in the overall CO + NO reaction. This study reports a kinetic investigation of the single CO + N_2O reaction on Rh/Al_2O_3, and on $Pt–Rh/Al_2O_3$, between 264 and 310 °C with inlet partial pressures in the range 3.4–13.8 × 10^{-3} and 1.5–5.9 × 10^{-3} atm respectively for CO and N_2O. Our mechanism proposal differs from those proposed earlier in the literature mainly by the dissociation step of chemisorbed N_2O species involving a nearest neighbor vacant site. The difference in the selectivity behavior toward the transformation of NO into N_2O on Pt and Rh has been related to competitive adsorptions between NO and N_2O. A comparison of the values of the equilibrium constant for the adsorption of N_2O with those earlier calculated for NO from the kinetic study of the CO + NO reaction on similar catalysts [J. Catal. 175 (1998) 194] shows that, on Pt, this competition is in favor of N_2O, which can readsorb and dissociate at low temperatures and low NO conversions. In contrast, the strongest NO adsorption on Rh inhibits the subsequent CO + N_2O reaction. In the second part of this study, the selected mechanism has been tentatively validated in a wider range of temperatures and conversions. The adsorbate coverage dependencies of the strength of the metal–adsorbate bond has been accounted for to model temperature-programmed conversion curves.

Keywords: Three-way catalyst; Kinetics of the CO + N_2O reaction; Pt- and Rh-based catalysts; $Pt–Rh/Al_2O_3$; Reaction mechanism; Nitrous oxide; N_2O selectivity

1. Introduction

Typically, the overall transformation of NO over automotive exhaust three-way catalysts obeys competitive and successive reactions involving the intermediate formation of N_2O:

$$2CO + 2NO \rightarrow N_2 + 2CO_2, \quad (1)$$

$$CO + 2NO \rightarrow N_2O + CO_2, \quad (2)$$

$$CO + N_2O \rightarrow N_2 + CO_2. \quad (3)$$

Nitrous oxide (N_2O) is an undesirable side product because of its greenhouse gas behavior. Currently, noble metal-based catalysts are efficient in selectively converting NO into N_2 under three-way conditions, except during the cold start, N_2O being the main N-containing product on Pt- and Rh-based catalysts. Further technological developments either to minimize the initial formation of N_2O or to enhance its subsequent reduction are of great interest. Among the different strategies already suggested for improving the selectivity toward the transformation of NO into N_2O, changes in the adsorption properties of noble metals (Pt and Rh) by various additives, such as ceria or lanthana, could be attractive [1–3]. Unfortunately, such modifications are mainly beneficial to the activity, whereas no significant improvement on the selectivity toward the production of N_2 is observed at least at low temperatures and conversions [4–8]. Hence, it seems obvious that a better understanding of the specific role of active phases, and of reaction mechanisms involved over automotive three-way catalysts (TWC), should bring crucial information for further practical applications.

Cho and co-workers [9–11] were one of the first to state the real importance of the subsequent reduction of N_2O during the overall transformation of NO. These authors suggested that the rate of N_2O conversion, formed during the partial reduction of NO, is sharply enhanced above the light-off temperature because of a lessening of the CO-inhibiting effect due to repulsive interactions between N_{ads} and CO_{ads}. Based on this suggestion, competitive adsorptions between

* Corresponding author.
E-mail address: pascal.granger@univ-lille1.fr (P. Granger).

0021-9517/$ – see front matter
doi:10.1016/j.jcat.2004.01.017

the reactants and the products on three-way catalysts could affect the selectivity behavior of noble metals. On this subject, comparative kinetic studies of the CO + NO and CO + N_2O reactions should bring relevant arguments for further discussions.

The kinetics of the overall CO + NO [12,13] and of the single CO + N_2O [14] reactions have been previously investigated in our laboratory mainly over noble metals. Regarding the kinetics of the CO + N_2O reaction on Pt/Al_2O_3, a mechanism scheme has been selected involving a neighbor vacant site for the dissociation step of chemisorbed N_2O molecules (step (6)),

$$CO + * \Longleftrightarrow CO_{ads}, \tag{4}$$

$$N_2O + * \Longleftrightarrow N_2O_{ads}, \tag{5}$$

$$N_2O_{ads} + * \rightarrow N_2 + O_{ads} + * \quad (\text{or } N_{2ads} + O_{ads}), \tag{6}$$

$$CO_{ads} + O_{ads} \rightarrow CO_2 + 2*, \tag{7}$$

where $*$ stands for a vacant adsorption site.

The rate Eq. (8) has been derived assuming competitive adsorption of the reactants at equilibrium, step (6) as rate determining, and CO and N_2O predominantly adsorbed on noble metals:

$$r_{N_2O} = \frac{k_6 \lambda_{N_2O} P_{N_2O}}{(1 + \lambda_{N_2O} P_{N_2O} + \lambda_{CO} P_{CO})^2}. \tag{8}$$

This rate equation differs from that established earlier by Belton and Schmieg [15] and Mac Cabe and Wong [16], respectively, on Rh/Al_2O_3 and Rh (111), who found more reliable correlations between experimental and calculated rates with

$$r_{N_2O} = \frac{k_{10} \lambda_{N_2O} P_{N_2O}}{1 + \lambda_{N_2O} P_{N_2O} + \lambda_{CO} P_{CO}}, \tag{9}$$

that takes into account no additional adsorption site for the dissociation of chemisorbed N_2O molecules according to

$$N_2O_{ads} \rightarrow N_2 + O_{ads}. \tag{10}$$

Cho and co-workers [9,10] also argued on the basis of Eq. (9) for explaining the rate enhancement of the subsequent reduction of N_2O on Rh above the light-off temperature.

The dissociative adsorption of N_2O can also be considered on Rh according to [17]

$$N_2O + * \rightarrow N_2 + O_{ads}. \tag{11}$$

In that case, the following rate Eq. (12), derived from a mechanism involving steps (4), (7), and (11), should be accounted for:

$$r_{N_2O} = \frac{k_{11} P_{N_2O}}{1 + \lambda_{CO} P_{CO}}. \tag{12}$$

k_6, k_{10}, and k_{11}, in Eqs. (8), (9), and (12), are respectively the rate constants of N_2O dissociation related to steps (6), (10), and (11), λ_i and P_i being respectively the equilibrium adsorption constant and the partial pressure of reactant i (i = CO, N_2O).

This paper deals with the kinetics of the CO + N_2O reaction on Rh/Al_2O_3 and on a bimetallic $Pt–Rh/Al_2O_3$ catalyst. The calculation of these kinetic and thermodynamic parameters and then their comparison with those previously estimated from the kinetic studies of the CO + NO reaction [12,13] on similar catalysts give arguments for explaining the changes in the selectivity behavior of Pt and Rh toward the production of N_2O. In the second part of this study, experimental and predicted rates have been compared in a wider range of temperatures and conversions.

2. Experimental

2.1. Catalysts

The catalyst preparation and characterization were described earlier [13]. Supported noble metal catalysts were prepared using a conventional coimpregnation of hexachloroplatinic acid and rhodium trichloride solutions with adjusted concentrations to obtain 1 wt% Pt and 0.2 wt% Rh. The impregnated solids were dried and calcined in air at 450 °C and then reduced in hydrogen at 450 °C for 2 h. According to the preparation procedure, the formation of bimetallic Pt–Rh particles is favored on $Pt–Rh/Al_2O_3$, rather than the segregation of Pt and Rh on alumina [18]. Additional infrared spectroscopic measurements of chemisorbed CO species on the metals evidenced the presence of surface Pt-enriched particles [19]. The residual chlorine content varied in the range 0.2–1.2 wt%. The metal dispersion, calculated from H_2 chemisorption at room temperature, using a pulse technique, assuming a H/M_s stoichiometry of 1 (with $M_s = Pt_s$ and/or Rh_s), were 0.93 and 0.64 respectively on Rh/Al_2O_3 and on $Pt–Rh/Al_2O_3$. The catalysts were in powder form with an average grain diameter of 80 μm.

2.2. Catalytic measurements

Details on the experimental setup were reported elsewhere [12]. Kinetic measurements were performed in a recycle fixed-bed flow reactor running under differential conditions, with a high recycle ratio of about 180. Preliminary steady-state experiments showed that the rate remained unchanged by modifying the catalyst loading, with a constant space velocity, indicating that external mass transfers were minimized. A rough estimation of the effectiveness factor by assuming a Knudsen regime, with an efficient coefficient of about 10^{-6} $m^2\,s^{-1}$, led to values close to 1 in our experimental conditions suggesting that internal diffusion phenomena, should not operate significantly [20]. Finally, the estimates of the Prater number in the range $2–3.4\times10^{-4}$, corresponding to a temperature deviation between the core and the surface of the grain less than 0.2 °C, suggested the achievement of a kinetic regime during rate measurements [21].

Typically, the catalyst loadings were 0.2 g mixed with 0.8 g of α-Al_2O_3. The total flow rate adjusted to 10 L h^{-1}

corresponded to a space velocity of 25,000 h^{-1}. Reactants and products were analyzed with a HP5890 Series II chromatograph fitted with a thermal conductivity detector. Prior to their quantification, N_2O, CO_2, CO, and N_2 were separated on a CTR1 column from Alltech. The specific rate was calculated according to

$$r_i = \frac{D_i \tau_i}{m} \quad \left(\mathrm{mol\,h^{-1}\,g^{-1}}\right), \tag{13}$$

where τ_i is the conversion, D_i the molar flow rate for the compound i, and m the mass of catalyst. The intrinsic rate, expressed per surface atom, was estimated based on the number of surface atoms calculated from H_2 chemisorption measurements.

3. Results

3.1. Previous temperature-programmed experiments

3.1.1. The single CO + N_2O reaction

Temperature-programmed experiments were performed under stoichiometric conditions with partial pressures of N_2O and CO equal to 5×10^{-3} atm. The conversion profiles in Fig. 1 obtained on Rh/Al_2O_3 and Pt–Rh/Al_2O_3 are compared with that previously obtained on Pt/Al_2O_3 [14]. The overall catalytic activity can be qualitatively compared from the light-off temperatures of respectively 295, 315, and 325 °C on 0.2 wt% Rh/Al_2O_3, 1 wt% Pt–0.2 wt% Rh/Al_2O_3, and 1 wt% Pt/Al_2O_3, corresponding to 50% N_2O conversion. This comparison underlines the higher activity of Rh/Al_2O_3 compared to Pt/Al_2O_3 which could be explained mainly by the higher intrinsic activity of Rh, the number of Pt surface atoms being higher than that of Rh over comparable weight sample, even though Pt dispersion is lower than that of Rh. Clearly, the intermediate conversions obtained on Pt–Rh/Al_2O_3 between those of Rh/Al_2O_3 and Pt/Al_2O_3 corroborate previous observations showing that Pt and Rh preserve their individual adsorption properties in surface Pt-enriched bimetallic particles [13].

3.1.2. The overall CO + NO reaction

Temperature-programmed reduction of NO by CO has been investigated on the same Rh/Al_2O_3 and Pt–Rh/Al_2O_3 catalysts under stoichiometric conditions with P_{NO} and P_{CO} of 5×10^{-3} atm. The conversion and selectivity profiles in Fig. 2 are compared with those previously obtained on Pt/Al_2O_3 [14]. NO light-off temperatures of respectively 262, 286, and 409 °C on Rh/Al_2O_3, Pt–Rh/Al_2O_3, and Pt/Al_2O_3 lead to the same reactivity sequence previously established for the single CO + N_2O reaction. Consequently, Rh/Al_2O_3 still exhibits the highest overall activity. Now regarding the selectivity behavior, it is obvious that the selectivity profile of Pt/Al_2O_3 differs from those obtained on Rh/Al_2O_3 and Pt–Rh/Al_2O_3. As observed in Fig. 2a, at low conversions (below the light-off temperature), S_{N_2O} gradually decreases on Pt/Al_2O_3 while it remains quasi-constant

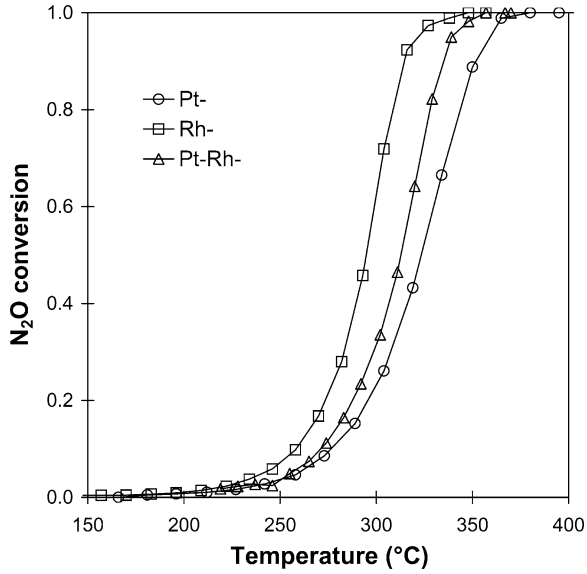

Fig. 1. Temperature-programmed conversion curves for the single CO + N_2O reaction under stoichiometric conditions with inlet partial pressures of CO and N_2O of 5×10^{-3} atm and a space velocity of 25,000 h^{-1}.

on Rh/Al_2O_3 and Pt–Rh/Al_2O_3 (Figs. 2b and 2c). It is also noticeable that the sharp decrease in S_{N_2O}, above the NO light-off temperature, when the subsequent CO + N_2O reaction becomes predominant, occurs at much higher conversion on Rh/Al_2O_3 and Pt–Rh/Al_2O_3 than on Pt/Al_2O_3. The difference is clear when comparing the conversion of NO where S_{N_2O} starts its sharp decrease: 40% for Pt/Al_2O_3, 80% for Pt–Rh/Al_2O_3, and 100% for Rh/Al_2O_3. Additional comparisons in Fig. 3, by plotting the conversion of NO into N_2O vs the overall conversion of NO can be obtained. A maximum in the production of N_2O, associated with the formation and the successive transformation of N_2O, shifting to higher NO conversion following the sequence Pt/Al_2O_3 < Pt–Rh/Al_2O_3 < Rh/Al_2O_3, is observed. Of course the influence of temperature should be taken into account for explaining such a tendency. However, the temperature effect on the selectivity changes is usually much less pronounced than on the activity. Based on these considerations, it seems obvious that the subsequent reduction of N_2O, during the overall CO + NO reaction, occurs more readily on Pt/Al_2O_3 than on Rh/Al_2O_3, Pt–Rh/Al_2O_3 exhibiting an intermediate selectivity behavior.

3.2. Steady-state kinetic measurements

3.2.1. Temperature dependency of the rate of the CO + N_2O reaction

Steady-state rate measurements were performed under stoichiometric conditions between 264 and 310 °C with inlet partial pressures of CO and N_2O of 6×10^{-3} atm. The values of the apparent activation energy calculated from the slopes of the Arrhenius plots in Fig. 4 are respectively equal to 137 and 133.6 kJ mol^{-1} on Rh/Al_2O_3 and Pt–Rh/Al_2O_3.

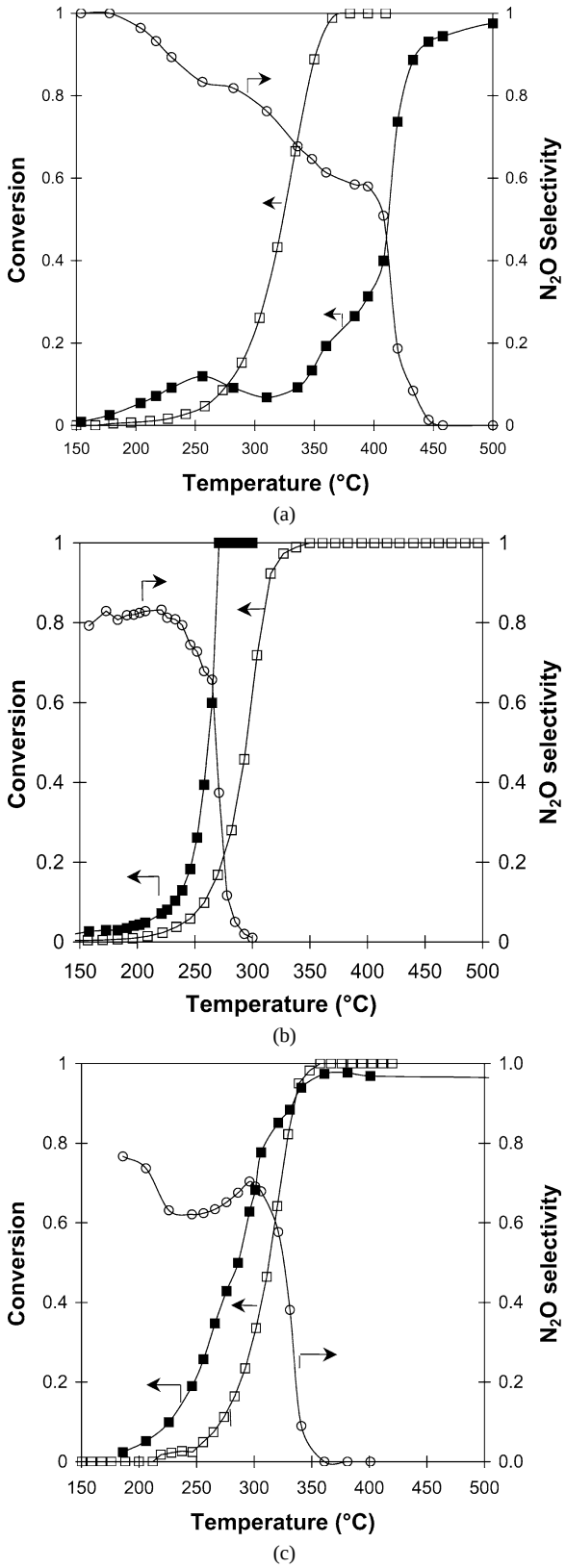

Fig. 2. Comparative temperature-programmed experiments of the $CO + N_2O$ and $CO + NO$ reactions under stoichiometric conditions: (○) N_2O selectivity in the $CO + NO$ reaction; (□) conversion of N_2O (in the single $CO + N_2O$ reaction); (■) conversion of NO on Pt/Al_2O_3 (a), on Rh/Al_2O_3 (b), on $Pt–Rh/Al_2O_3$ (c).

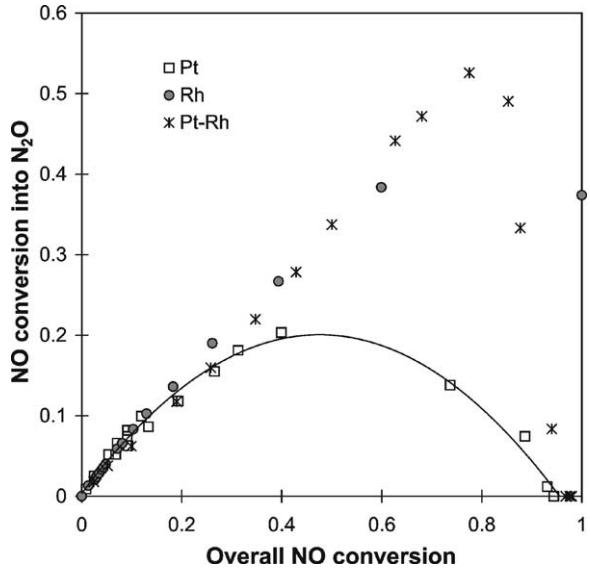

Fig. 3. Plots of the conversion of NO into N_2O as a function of the overall NO conversion during the $CO + NO$ reactions with $P_{NO} = P_{CO} = 5 \times 10^{-3}$ atm on Pt/Al_2O_3, Rh/Al_2O_3, and $Pt–Rh/Al_2O_3$.

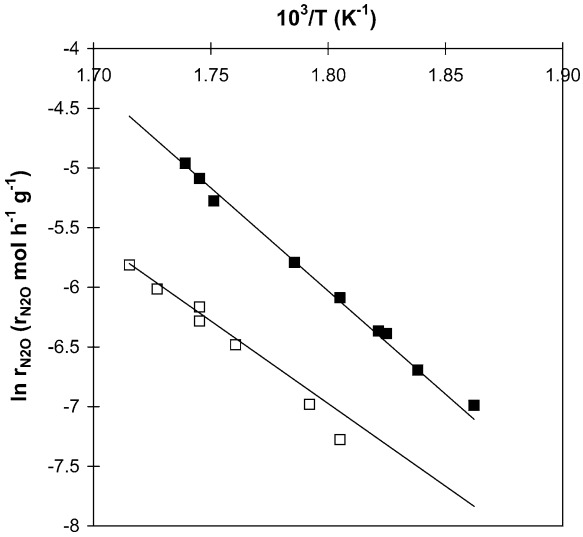

Fig. 4. Arrhenius plots for the $CO + N_2O$ reaction on Rh/Al_2O_3 (■) and $Pt–Rh/Al_2O_3$ (□) under stoichiometric conditions with inlet partial pressures of CO and N_2O of 6×10^{-3} atm. Predicted curves calculated from Eq. (16) (—).

3.2.2. Partial pressure dependencies of the rate of N_2O transformation

The influence of the reactant partial pressures (P_{CO} and P_{N_2O}) on the rate was investigated at 300 °C in the range 3.4–13.8×10^{-3} and 1.5–5.9×10^{-3} atm for CO and N_2O, respectively. Figs. 5 and 6 illustrate the influence of the partial pressure of N_2O and CO on the rate of the $CO + N_2O$ reaction, at constant P_{CO} and P_{N_2O}, respectively. The values for the apparent average kinetic orders with respect to the partial pressure of N_2O are 0.75 ± 0.11 and 0.71 ± 0.11 on Rh/Al_2O_3 and on $Pt–Rh/Al_2O_3$, while the negative values obtained for the CO order, respectively equal to

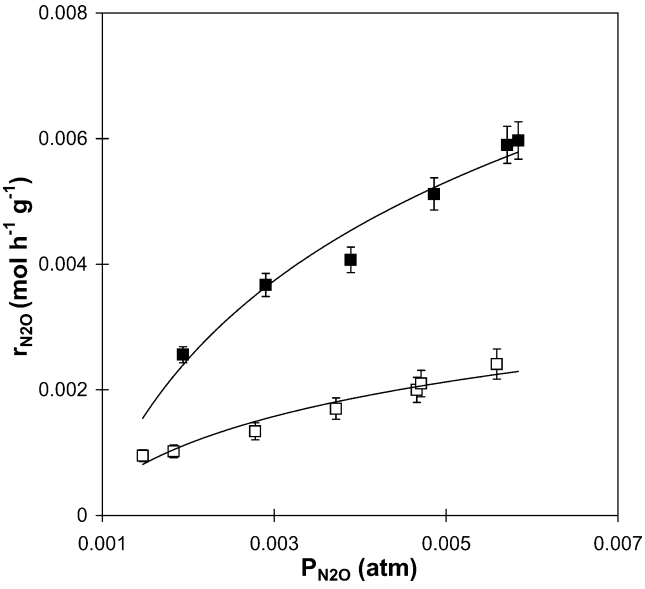

Fig. 5. N_2O partial pressure dependency of the rate of the $CO + N_2O$ reaction at 300 °C on Rh/Al_2O_3 (■) and on $Pt–Rh/Al_2O_3$ (□). Inlet $P_{CO} = 6 \times 10^{-3}$ atm.

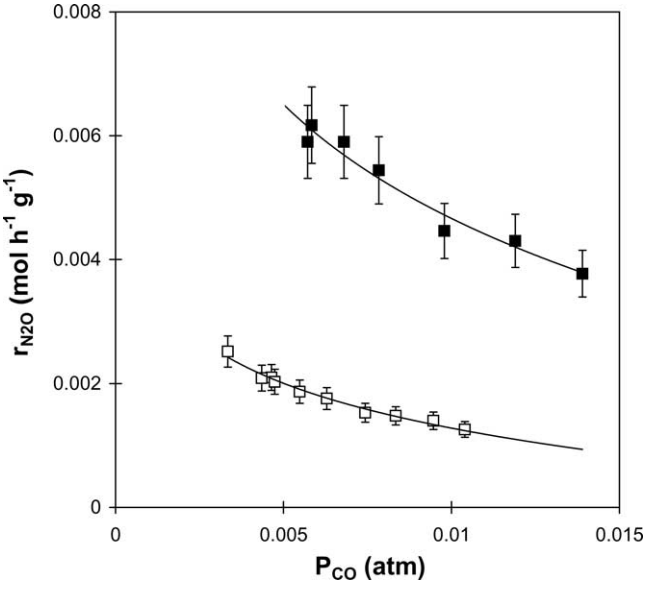

Fig. 6. CO partial pressure dependency of the rate of the $CO + N_2O$ reaction at 300 °C on Rh/Al_2O_3 (■) and on $Pt–Rh/Al_2O_3$ (□). Inlet $P_{N_2O} = 6 \times 10^{-3}$ atm.

-0.54 ± 0.08 and -0.58 ± 0.09, reflect the well-known CO-inhibiting effect on the reaction rate. These reaction orders are in qualitative agreement with those reported in the literature [15,16].

4. Discussion

Currently, there is a general agreement on the mechanism scheme for displaying the $CO + NO$ reaction over noble metals, whereas some divergences arise in the case of the $CO + N_2O$ reaction, particularly on Rh. Previous investigations on the kinetics of the $CO + NO$ reaction highlighted the beneficial effect of rhodium, dissociating NO more easily than platinum [22,23], and also the structure sensitivity of such a reaction [23–25]. In the case of the single $CO + N_2O$ reaction, comparisons in Fig. 1 also indicate that rhodium is more active than Pt in the transformation of N_2O, in accordance with previous results obtained for the transformation of N_2O the presence and/or in the absence of CO [26].

Currently, there is no general agreement on the mechanism of the $CO + N_2O$ reaction, the involvement of a dissociative adsorption, or a twostep mechanism involving molecular adsorption and dissociation steps, being questionable on Rh. In this latter case, the involvement of a nearest neighbor site could also be considered. In a previous investigation performed in our laboratory, it was found that the mechanism, noted in the Introduction, is the most representative on Pt/Al_2O_3 for depicting the single $CO + N_2O$ reaction. Alternately, previous workers [10,11,15,16] disagree with step (6) on Rh, and rather propose step (9) ($N_2O_{ads} \rightarrow N_2 + O_{ads}$). Consequently molecular or dissociative adsorption for N_2O could be equally considered on Rh, as well as the requirement or not of an additional nearest neighbor vacant site for the dissociation of chemisorbed N_2O molecules.

The clarification of the mechanism of the $CO + N_2O$ is of interest for further explaining the formation and the subsequent transformation of N_2O during the reduction of NO by CO. As illustrated in Figs. 2 and 3, it seems obvious that the subsequent $CO + N_2O$ reaction in the presence of NO, occurs more readily on Pt/Al_2O_3 than on Rh/Al_2O_3 and $Pt–Rh/Al_2O_3$ despite the fact that Rh/Al_2O_3 is more active in converting N_2O than Pt/Al_2O_3 in the absence of NO (see Fig. 1). Such a discrepancy could be equally explained by differences in the ability of Pt and Rh to dissociate N_2O, or by different properties toward the adsorptions of CO, NO, and N_2O, when they compete in accordance with previous authors [10,11,27].

4.1. On supported Rh catalysts

In this section, kinetic data obtained on Rh/Al_2O_3 have been interpreted on the basis of previous findings mainly obtained on rhodium-based catalysts [15,16], and those obtained more recently in our laboratory on Pt/Al_2O_3 [14]. First, we have attempted to check for Rh/Al_2O_3 the validity of the mechanism earlier established for Pt/Al_2O_3.

No relevant conclusion can be drawn from the comparable CO order values of respectively -0.51 and -0.54 on Pt/Al_2O_3 and Rh/Al_2O_3. They underline the usual CO-inhibiting effect on the rate of N_2O transformation that can be modeled either by Eqs. (8), (9), or (12). On the other hand, the examination of the apparent N_2O order value on Rh/Al_2O_3, invalidates Eq. (12) which only assumes a value equal to one. Consequently, the occurrence of a dissociative adsorption of N_2O, via step (11), seems to be unlikely on Rh/Al_2O_3. Let us now examine a two-step mechanism with a

Table 1
Comparison of kinetic and thermodynamic parameters for the $CO + N_2O$ reaction calculated on Rh/Al_2O_3 at 300 °C

Reaction	α_i [a]		β_i [b]		λ_{CO}	λ_{N_2O}	k'_n	Residual sum
step	$i = CO$	$i = N_2O$	$i = CO$	$i = N_2O$	(atm^{-1})	(atm^{-1})	(10^2 mol h^{-1} at_s^{-1})	of square
(6)	34.15	31.0	0.78	0.82	70 ± 25	53 ± 16	88.9 ± 26.7	
					54 ± 16	42 ± 13	261.5 ± 78.5	
					50 ± 8 [c]	36 ± 6 [c]	34 ± 5.1 [c]	7.86×10^{-8}
(10)	75.4	57.7	0.51	0.66	268 ± 80	350 ± 105		
					335 ± 100	438 ± 131		
					194 ± 29 [c]	113 ± 17 [c]	41.8 ± 6.3 [c]	10.5×10^{-8}

[a] Slopes of the linear plots $\sqrt{P_{N_2O}P_{CO}/r_{CO}}$, $\sqrt{P_{N_2O}/r_{CO}}$, P_{N_2O}/r_{CO} vs P_{N_2O} and P_{CO}.
[b] Intercepts of the linear plots $\sqrt{P_{N_2O}P_{CO}/r_{CO}}$, $\sqrt{P_{N_2O}/r_{CO}}$, P_{N_2O}/r_{CO} vs P_{N_2O} and P_{CO}.
[c] Adjusted values from the statistical method.

dissociation of molecular chemisorbed N_2O species involving or not an additional site. In that case, the corresponding rate Eqs. (8) and (9) can be linearized leading respectively to

$$\sqrt{\frac{P_{N_2O}}{r_{N_2O}}} = \frac{1 + \lambda_{N_2O}P_{N_2O} + \lambda_{CO}P_{CO}}{\sqrt{k_6\lambda_{N_2O}}}, \tag{14}$$

$$\frac{P_{N_2O}}{r_{N_2O}} = \frac{1 + \lambda_{N_2O}P_{N_2O} + \lambda_{CO}P_{CO}}{k_{10}\lambda_{N_2O}}. \tag{15}$$

In both cases, linear plots P_{N_2O}/r_{N_2O} and $\sqrt{P_{N_2O}/r_{N_2O}}$ versus P_{N_2O} or P_{CO} are obtained. A mechanism has been tentatively selected by comparing the parameters k_n and λ_i estimated from the intercepts β_i and the slopes α_i of the straight lines. Unfortunately the calculations, summarized in Table 1, lead to positive values in both cases and thus cannot discriminate between steps (6) and (10). On the other hand, the comparison of the values of λ_{CO} obtained in this study, with those previously estimated from the kinetic investigation of the $CO + NO$ reaction on the same catalyst [13], could be relevant since comparable values should be obtained. According to the margin of error, the estimates of λ_{CO}, using Eq. (8), are in good agreement with the optimized value of $\lambda_{CO} = 71$ atm^{-1} earlier obtained for the $CO + NO$ reaction [13], whereas the numerical solutions obtained from Eq. (9) diverge. Such a discrimination can also be achieved using the solver setup on Excel 5 from Microsoft by minimizing the square differences between experimental and calculated rates using Eqs. (8) and (9). The optimization routine, described elsewhere [13], leads to a better adjustment from Eq. (8) with a lower residual sum of squares. In addition, a better agreement between the set of values obtained from the optimization and the graphical procedure is obtained using Eq. (8). Consequently, the results obtained from both methods seem to be in better agreement with the fact that the mechanism earlier described on Pt/Al_2O_3, involving a nearest neighbor vacant site for the dissociation of chemisorbed N_2O molecules (step (6)), is still the most representative on Rh/Al_2O_3. Such a proposal seems consistent with previous surface science studies which showed that the adsorption and the subsequent dissociation of N_2O on Rh (111) necessitate geometrical requirements [28]. Earlier investigations found that the orientation of adsorbed N_2O molecules over metallic sites could have an influence on the further elementary steps [28–30]. If N_2O chemisorbs via the terminal N atom, its subsequent dissociation is likely to necessitate a neighbor free adsorption site. On the contrary, if N_2O is coordinated via the oxygen atom, then the dissociation could take place without an additional site. As a matter of fact theoretical calculations performed in our laboratory over monometallic and bimetallic Pt and Rh clusters [31], based on the density functional theory, showed that N_2O adsorbs via the terminal N atom, whereas the configuration with N_2O bound to the metal via the oxygen is thermodynamically unstable over noble metals. Hence, both theoretical and kinetic results obtained in our laboratory speak in favor of molecular N_2O adsorption, and subsequent dissociation of N_2O involving active sites. Such a result is in line with conclusions of previous authors who suggested that the dissociation of N_2O on Ru (001) necessitates at least four bare Ru atoms [27].

The comparison of the optimized values for λ_i and k'_n on Pt/Al_2O_3 and Rh/Al_2O_3, in Table 2, shows slight changes in λ_{N_2O} while λ_{CO} does not significantly vary probably within the margin of error. As far as the intrinsic rate of N_2O dissociation (k'_6) is concerned, only slight variations are observable (3400 on Rh/Al_2O_3 against 1000 molec h^{-1} at_s^{-1} on Pt/Al_2O_3). Nevertheless, they could reflect changes in the reactivity of chemisorbed N_2O molecules on Rh and Pt. Such a statement is supported by theoretical calculations [31], which show that modifications in the geometrical configurations of chemisorbed N_2O species on Pt and Rh. N_2O, coordinated to Pt, are upright, while bent N_2O molecules, bonded with two adjacent Rh atoms, are stabilized on Rh clusters. Such changes in configurations lead to a weakening of the terminal N–O bond being more accentuated on Rh than on Pt. Hence, these results corroborate our kinetic data showing that the dissociation of the N–O bond in N_2O molecules is easier on Rh/Al_2O_3 than on Pt/Al_2O_3.

The comparison between λ_i calculated for the single $CO + N_2O$ reaction with those previously estimated for the $CO + NO$ reaction on Pt/Al_2O_3 and Rh/Al_2O_3 is interesting because it could explain changes in selectivity for the $CO + NO$ reaction (Figs. 2 and 3). In the overall $CO + NO$

Table 2
Comparison of the kinetic and thermodynamic data obtained at 300 °C for the CO + NO and CO + N_2O reactions

Catalyst	Reaction	P_{CO} (10^{-3} atm)	P_{NO} or P_{N_2O} (10^{-3} atm)	λ_{NO} or λ_{N_2O} (atm^{-1})	λ_{CO} (atm^{-1})	k'_n [a] (10^2 mol h^{-1} at_s^{-1})
Pt/Al_2O_3	CO + NO	5–9	1.5–5.6	11 ± 2	121 ± 18	4.0 ± 0.6
	CO + N_2O	3.6–13.8	1.8–7.4	90 ± 13	78 ± 12	10.0 ± 1.5
Rh/Al_2O_3	CO + NO	3–13.6	0.5–3.2	472 ± 71	71 ± 11	123.1 ± 18.5
	CO + N_2O	3.6–13.8	1.8–7.4	36 ± 6	50 ± 8	34.0 ± 5.1
Pt–Rh/Al_2O_3	CO + NO	3–8	1.5–5.6	505 ± 76	122 ± 18	2.8 ± 0.4
	CO + N_2O	3.8–10.4	1.5–5.6	66 ± 10	91 ± 14	4.2 ± 0.6

[a] Intrinsic rate constant for the dissociation step of N_2O ($N_2O_{ads} + * \rightarrow N_2 + O_{ads} + *$) and of NO ($NO_{ads} + * \rightarrow N_{ads} + O_{ads}$) in the mechanism of the CO + N_2O and CO + NO reactions.

reaction, the initial selectivity toward the transformation of NO into N_2O depends on the relative rates of reactions (1) and (2), while at higher conversions, S_{N_2O} is also affected by the subsequent reduction of N_2O via reaction (3). The differences in the selectivity behavior of Pt and Rh are very well explained by comparing the values obtained for λ_{N_2O} and λ_{NO}, λ_{N_2O} being approximately one order of magnitude higher than λ_{NO} on Pt/Al_2O_3; consequently, this can explain the better reactivity of N_2O, since its surface coverage is higher than that of NO. Such a difference in adsorption behavior could also satisfactorily explain the changes of S_{N_2O} in the CO + NO reaction on Rh/Al_2O_3, N_2O, initially formed on Rh/Al_2O_3, which can hardly adsorb because of its much lower λ_{N_2O} compared with λ_{NO}. The reverse tendency is observed on Pt, because λ_{NO} is significantly much lower than λ_{N_2O}. In such a case, N_2O can be adsorbed even in the presence of NO and further dissociate, explaining the faster decrease of S_{N_2O} on Pt than on Rh.

4.2. On supported bimetallic Pt–Rh catalysts

With regard to Pt–Rh/Al_2O_3, two borderline cases can be envisaged because of competitive adsorptions of the reactants or not. Such a suggestion is supported by previous kinetic and spectroscopic investigations of the CO + NO reaction respectively on Pt–Rh/Al_2O_3 [12], and on Pt–Rh/SiO_2 [32]. In the former case, noncompetitive adsorptions of NO and CO were concluded based on the comparison of λ_{NO} and λ_{CO} on Pt/Al_2O_3 and Rh/Al_2O_3, λ_{NO} being substantially higher on Rh than on Pt, while the reverse trend was observed on Pt/Al_2O_3 for λ_{CO}. The values reported in Table 2 show only slight differences on the estimates of λ_{N_2O} and λ_{CO} on Pt/Al_2O_3 and Rh/Al_2O_3. Accordingly, competitive adsorptions of N_2O and CO seem more probable on Pt–Rh/Al_2O_3, Eq. (8) being still valid for depicting the reactant partial pressure dependencies of the rate of N_2O reduction on Pt–Rh/Al_2O_3 at 300 °C. The parameters k'_6 and λ_i have been calculated at that temperature using procedures similar to those applied for monometallic catalysts. The adjustment routine leads to average values for λ_{N_2O} between those calculated on Pt/Al_2O_3 and Rh/Al_2O_3 (see Table 2). However, it is worthwhile to note that the optimized values for k'_6 and λ_{N_2O} on Pt–Rh/Al_2O_3 are closer to those obtained on Pt/Al_2O_3 than on Rh/Al_2O_3. Such a comparison corroborates previous results indicating that Pt–Rh/Al_2O_3 is a surface Pt-enriched catalyst.

Now regarding the selectivity toward the transformation of N_2O, Fig. 3 shows that the selectivity behavior of Pt–Rh/Al_2O_3 is closer to that of Rh/Al_2O_3 than that of Pt/Al_2O_3. As illustrated in Fig. 3, the subsequent CO + N_2O reaction becomes significant above 80% NO conversion on Pt–Rh/Al_2O_3 and Rh/Al_2O_3, whereas it occurs at much lower NO conversion on Pt/Al_2O_3. According to previous comparison on Rh, such kinetic features on Pt–Rh/Al_2O_3 can easily be explained by the difference in the equilibrium adsorption constant of NO and N_2O (see Table 2). This comparison indicates that competitive adsorption is still in favor of NO on Pt–Rh/Al_2O_3. Consequently, N_2O can readsorb and then decompose when NO is quasi-completely depleted from the surface near 100% NO conversion.

In our case, the previous explanations suggested earlier by Cho do not seem to be adequate since only slight variations in λ_{CO} are observed, probably varying within the margin of error. According to Cho's statements, the adjusted values of λ_{CO} should be lower in the case of the CO + NO, accounting for repulsive interactions between N_{ads} and CO_{ads}, than those calculated from the single CO + N_2O, the dissociation of the N–N bond being not thermodynamically favored in N_2O molecules. In fact, the results in Table 2 show the reverse trend, the lowest values being systematically obtained from the CO + N_2O reaction.

4.3. Simulation of temperature-programmed experiments under stoichiometric conditions

In a previous paper an attempt for modeling the CO + N_2O on Pt/Al_2O_3 under three-way conditions, near 100% N_2O conversion, is reported [14]. Temperature-programmed (TP) conversion curves can be predicted under differential conditions using

$$r_{N_2O} = \frac{D_{N_2O}\tau_{N_2O}}{m} = \frac{k_6\lambda_{N_2O}(1-\tau_{N_2O})P^0_{N_2O}}{(1+\lambda_{N_2O}(1-\tau_{N_2O})P^0_{N_2O}+\lambda_{CO}(1-\tau_{CO})P^0_{CO})^2}, \quad (16)$$

P^0_i is the inlet partial pressure of N_2O.

Table 3
Comparison of the adjusted kinetic and thermodynamic parameters for the $CO + N_2O$ reaction on monometallic and bimetallic Pt- and Rh-based catalysts

Catalyst	Preexponential factor			Adsorption enthalpy [b]		Activation energy [c]
	A (10^9 s^{-1})	f_{CO} (10^{-2} atm^{-1})	f_{N_2O} (10^{-2} atm^{-1})	$\Delta H_{ads,CO}$	$\Delta H_{ads,N_2O}$	E (kJ mol^{-1})
Pt/Al_2O_3 [a]	4.1 ± 0.6	12.0 ± 1.8	5.2 ± 0.8	-28.6 ± 4.3	-34.3 ± 5.2	112 ± 17
Rh/Al_2O_3	650 ± 98	1.4 ± 0.2	64 ± 10	-39.1 ± 6.0	-19.3 ± 2.9	130.3 ± 19.5
$Pt–Rh/Al_2O_3$	3.9 ± 0.6	10.0 ± 1.5	6.3 ± 1.0	-32.5 ± 4.9	-33.3 ± 5.0	117.7 ± 17.7

[a] See Ref. [14].
[b] In kJ mol^{-1}.
[c] Related to step (6).

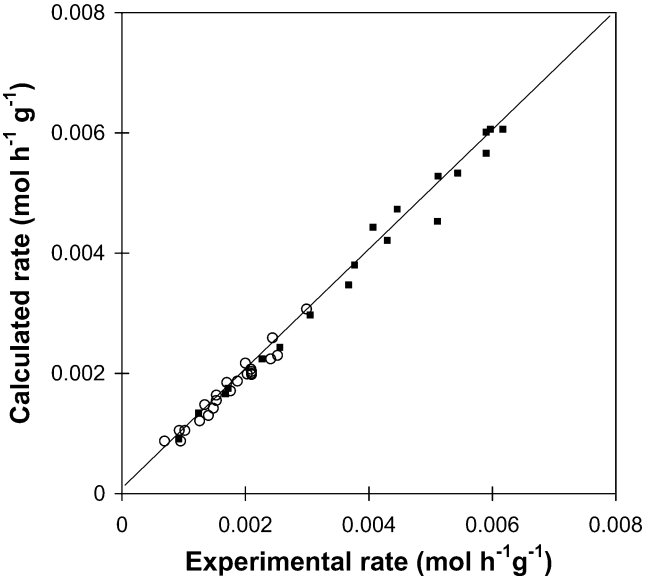

Fig. 7. Correlation between experimental and calculated rates on Rh/Al_2O_3 (■) and on $Pt–Rh/Al_2O_3$ (○).

Typically, the simulation of temperature-programmed conversion curves consists in quantifying the temperature dependency of the rate constant k_6, related to step (6), and of the equilibrium constants for CO and N_2O adsorptions according to Eqs. (17) and (18). The parameters A and f_i, the preexponential factors of respectively k_6 and λ_i, E the activation energy related to step (6), and $\Delta H_{ads,i}$ the adsorption enthalpy of the reactant i have been optimized from steady-state rate measurements performed at low conversion in Figs. 4–6. The adjusted values for these different parameters are collected in Table 3. Fig. 7 shows a good fit between experimental and calculated rates from Eqs. (8), (17), and (18).

$$k_6 = A \exp\left(-\frac{E}{RT}\right) \quad \text{and} \tag{17}$$

$$\lambda_i = f_i \exp\left(-\frac{\Delta H_{ads,i}}{RT}\right) \quad \text{with } f_i = \exp\left(\frac{\Delta S_{ads,i}}{R}\right). \tag{18}$$

However, divergences were found between experimental and calculated TP conversion curves using the optimized values of the adsorption enthalpies for CO and N_2O adsorption in Table 3. Such discrepancies have not been related to significant heat and mass-transfer restrictions during temperature-programmed experiments, but mainly to changes in adsorption properties of noble metals during the temperature-programmed $CO + N_2O$ reaction. Typically, deactivation phenomena could alter differently the surface properties of noble metals with the buildup of oxygen species yielding electrophilic sites [33]. In the particular case of Rh-based catalysts, the well-known oxidative-disruption/reductive agglomeration could alter the adsorption properties of Rh particles [34]. Alternately, the accumulation of adsorbates can also change the adsorption properties of noble metals. Such a statement is supported by previous CO chemisorption measurements performed on $Pt–Rh/Al_2O_3$ [35], which showed a weakening of the metal–CO bond with an increase in CO coverage. Such an observation is in line with previous surface science studies explaining such an effect by a lessening of the electron back-donation into the π^* antibonding molecular orbital of CO, or lateral repulsive interactions between adsorbed CO molecules mainly at high CO coverage [36,37]. Such a surface coverage dependency of CO adsorption on $Pt–Rh/Al_2O_3$ has been modeled using Freundlich's assumptions [35], $\Delta H_{ads,CO}$ being a linear function of ln n_{CO} on $Pt–Rh/Al_2O_3$ (n_{CO} stands for the amount of adsorbed CO molecules at a given P_{CO}). According to these previous observations, semilogarithmic relationship have also been considered for modeling changes in $\Delta H_{ads,i}$ during temperature-programmed experiments of the $CO + NO$ and of the $CO + N_2O$ reactions respectively on $Pt–Rh/Al_2O_3$ [35] and Pt/Al_2O_3 [12]. The influence of the partial pressures of CO and N_2O (i.e., the surface coverage) on $\Delta H_{ads,i}$ can be modeled by empirical equations which account for mutual interactions involving only CO, and only N_2O molecules, or either N_2O or CO molecules. The extent of such interactions depends on the N_2O and CO coverages and therefore on the partial pressure ratio P_{N_2O}/P_{CO}:

$$\Delta H_{ads,N_2O} = a_{N_2O} + b \ln P_{N_2O} + c \ln P_{CO}, \tag{19}$$

$$\Delta H_{ads,CO} = a_{CO} + b' \ln P_{N_2O} + c' \ln P_{CO}. \tag{20}$$

Under stoichiometric conditions, $P_{N_2O} = P_{CO} = P_i$, then Eqs. (19) and (20) can be simplified, leading to

$$\Delta H_{ads,N_2O} = a_{N_2O} + b_{N_2O} \ln P_i, \tag{21}$$

$$\Delta H_{ads,CO} = a_{CO} + b_{CO} \ln P_i. \tag{22}$$

The parameters E, a_i, and b_i and the preexponential factor A and f_i have been adjusted on Rh/Al_2O_3 and $Pt–Rh/Al_2O_3$ by comparing experimental and predicted TP con-

Table 4
Influence of partial pressures of the reactants on the adsorption enthalpies of CO and NO over supported Pt- and Rh-based catalysts

Catalyst	A (10^9 s^{-1})	E (kJ mol^{-1})	Adsorbate	f_i [a] (10^{-2} atm^{-1})	a_i (kJ mol^{-1})	b_i (kJ mol^{-1})
Pt/Al_2O_3 [b]			N_2O	6.4 ± 1.0	-12.2 ± 1.8	3.9 ± 0.6
			CO	18.0 ± 2.7	-2.8 ± 0.4	5.0 ± 0.8
Rh/Al_2O_3	550 ± 82	131.8 ± 19.8	N_2O	7.0 ± 1.0	-10.1 ± 1.5	4.0 ± 0.6
			CO	5.0 ± 0.8	-16.7 ± 2.5	1.7 ± 0.3
$Pt–Rh/Al_2O_3$	2.0 ± 0.3	110.1 ± 16.5	N_2O	11.2 ± 1.7	-7.3 ± 1.1	4.0 ± 0.6
			CO	93 ± 14	-13.6 ± 2.1	1.3 ± 0.2

[a] $\lambda_i = f_i \exp[-\Delta H_{\mathrm{ads},i}/RT]$ (atm^{-1}) with $f_i = \exp[\Delta S_{\mathrm{ads},i}/R]$.
[b] See Ref. [14]

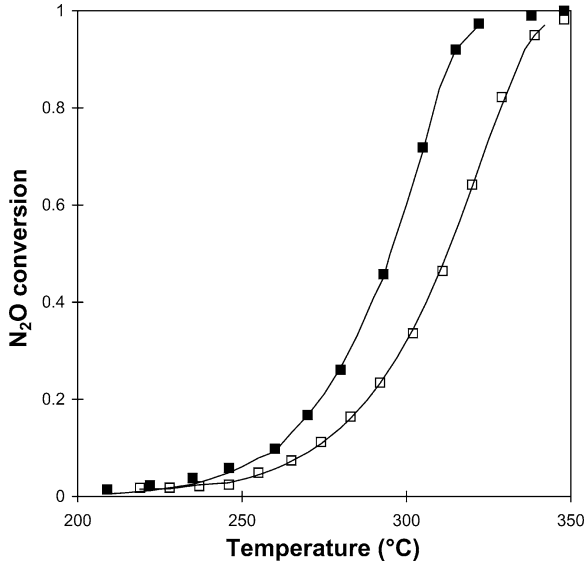

Fig. 8. Comparison between experimental and predicted N_2O conversion curves vs temperature from temperature-programmed experiments performed under stoichiometric conditions on Rh/Al_2O_3 (■) and $Pt–Rh/Al_2O_3$ (□); (—) predicted curves.

versions using Eq. (16). As observed in Fig. 8, the results in Table 4 lead to a good correlation between experimental and calculated conversions, except at quasi-complete conversion when P_i tends toward 0. Under such conditions, the numerical solutions from Eqs. (21) and (22) diverge, both equations being invalid when $P_i = 0$. As seen in Table 4, the optimized values for a_{CO} and $a_{\mathrm{N_2O}}$ are still in agreement with previous trends, observed in Table 3, demonstrating that N_2O still adsorbs more strongly on Pt/Al_2O_3 than on Rh/Al_2O_3 near saturation. Finally, both results show that a rate expression derived from a selected mechanism, accounting for adsorbate coverage dependencies of the adsorption enthalpies, can be profitably used for modeling light-off curves on three-way catalysts.

5. Conclusion

The kinetics of the $CO + N_2O$ reaction has been investigated on Rh/Al_2O_3 and $Pt–Rh/Al_2O_3$. The mechanism selected involves a dissociation of chemisorbed N_2O molecules on nearest neighbor vacant sites according to previous findings on Pt/Al_2O_3. The estimation of the equilibrium constants of N_2O, CO and of the rate constant of N_2O dissociation on Pt and Rh and their comparison suggests that CO and N_2O compete for adsorption on $Pt–Rh/Al_2O_3$ and that N_2O dissociates more readily on Rh/Al_2O_3. Additional comparisons with the equilibrium constants for CO and NO adsorption previously calculated from the kinetics of the $CO + NO$ reaction give arguments for explaining changes in selectivity toward the formation of N_2O particularly during the cold start. It appears that competitive adsorptions between NO and N_2O govern the selectivity behavior of Pt and Rh. Strongly chemisorbed NO species on Rh would prevent the readsorption of N_2O, initially formed, and its subsequent dissociation. On the other hand, such a competition is in favor of N_2O on Pt. Such a difference in adsorption properties correctly explains the most interesting selectivity toward the production of N_2 on Pt/Al_2O_3. Correlations between predicted and experimental temperature-programmed conversion curves can be achieved by taking into account the surface coverage dependency of $\Delta H_{\mathrm{ads},i}$.

References

[1] J. Cunningham, J.N. Hickey, R. Cataluna, J.C. Conesa, J. Soria, A. Martinez-Arias, Stud. Surf. Sci. Catal. 101 (1996) 681.
[2] J.H. Holles, M.A. Switzer, R.J. Davis, J. Catal. 190 (2000) 247.
[3] N.T. Pande, A.T. Bell, J. Catal. 98 (1986) 7.
[4] P. Granger, J.-F. Lamonier, N. Sergent, A. Aboukais, L. Leclercq, G. Leclercq, Top. Catal. 16/17 (2001) 89.
[5] P. Fornasiero, N. Hickey, J. Kaspar, T. Montini, M. Graziani, J. Catal. 189 (2000) 339.
[6] R. Di Monte, P. Fornasiero, J. Kaspar, P. Rumori, G. Gubitosa, M. Graziani, Appl. Catal. B 24 (2000) 157.
[7] D. Ciuparu, A. Bensalem, L. Pfefferle, Appl. Catal. B 26 (2000) 241.
[8] P. Granger, L. Delannoy, J.-J. Lecomte, C. Dathy, H. Praliaud, L. Leclercq, G. Leclercq, J. Catal. 207 (2002) 202.
[9] B.K. Cho, B.H. Shanks, J.E. Bailey, J. Catal. 115 (1989) 486.
[10] B.K. Cho, J. Catal. 138 (1992) 255.
[11] B.K. Cho, J. Catal. 148 (1994) 697.
[12] P. Granger, J.-J. Lecomte, C. Dathy, L. Leclercq, G. Mabilon, M. Prigent, G. Leclercq, J. Catal. 173 (1998) 304.
[13] P. Granger, J.-J. Lecomte, C. Dathy, L. Leclercq, G. Leclercq, J. Catal. 175 (1998) 194.
[14] P. Granger, P. Malfoy, P. Esteves, L. Leclercq, G. Leclercq, J. Catal. 187 (1999) 321.

[15] D.N. Belton, S.J. Schmieg, J. Catal. 138 (1992) 70.
[16] R.W. Mac Cabe, C. Wong, J. Catal. 121 (1990) 422.
[17] R.R. Sadhankar, J. Ye, D.T. Lynch, J. Catal. 146 (1994) 511.
[18] S. Kacimi, D. Duprez, in: A. Crucq (Ed.), in: Catalysis and Automotive Pollution Control II, vol. 71, Elsevier, Amsterdam, 1991, p. 581.
[19] P. Granger, L. Delannoy, L. Leclercq, G. Leclercq, J. Catal. 177 (1998) 147.
[20] P. Trambouze, H. Van Landeghem, J.-P. Wauquier, Les réacteurs chimiques, conception, calcul, mise en oeuvre, Technip, Paris, 1984.
[21] J.-F. Lepage, J. Cosyns, P. Courty, E. Freund, J.-P. Franck, Y. Jacquin, B. Juquin, C. Marcilly, G. Martino, J. Miquel, R. Montarnal, A. Sugier, H. Van Landeghem, Catalyse de contact, Technip, Paris, 1978.
[22] R.J. Gorte, L.D. Schmidt, J.L. Gland, Surf. Sci. 109 (1981) 367.
[23] D.T. Wickham, B.A. Banse, B.E. Koel, Surf. Sci. 243 (1991) 83.
[24] S.W. Jorgensen, N.D.S. Canning, R.J. Madix, Surf. Sci. 179 (1987) 322.
[25] D. Loffreda, D. Simon, P. Sautet, J. Catal. 213 (2003) 211.
[26] P. Malfoy, P. Granger, J.-F. Lamonier, L. Leclercq, G. Leclercq, Phys. Chem. 41 (1997) 109.
[27] H.H. Huang, C.S. Seet, Z. Zou, G.Q. Xu, Surf. Sci. 356 (1996) 181.
[28] Y. Li, M. Bowker, Surf. Sci. 348 (1996) 67.
[29] V.P. Zhdanov, J. Catal. 162 (1996) 47.
[30] A.A. Diamantis, G.J. Sparrow, J. Colloid Interface Sci. 47 (1974) 455.
[31] P. Granger, P. Malfoy, P. Esteves, J.-F. Paul, L. Leclercq, G. Leclercq, Europacat IV, Book of Abstracts, Rimini, 1999.
[32] R.F. van Slooten, B.E. Nieuwenhuys, J. Catal. 100 (1986) 360.
[33] Y.J. Mergler, B.E. Nieuwenhuys, J. Catal. 161 (1996) 292.
[34] F. Solymosi, M. Pasztor, J. Phys. Chem. 89 (1985) 4789.
[35] P. Granger, J.-J. Lecomte, L. Leclercq, G. Leclercq, Appl. Catal. A 208 (2001) 369.
[36] E.G. Seebauer, A.C.F. Kong, L.D. Schmidt, Surf. Sci. 176 (1986) 134.
[37] G. Ertl, M. Neuman, K.M. Streit, Surf. Sci. 64 (1977) 393.